Numerical modelling of interaction between the atmospheric boundary layer and the Antarctic ice shelf

V. N. LYKOSSOV*

Abstract — Using the data of observations of the ice cover in the Weddell Sea near the Antarctic coast in a period of the polar night, we carried out numerical experiments with the one-dimensional model of the atmospheric boundary layer. The processes of background advective heat and moisture transport, the catabatic component of motions and vertical turbulent snow transport under the conditions of blowing snow are parameterized in the model. It is shown that the results on the computation of temperature and specific humidity are in good agreement with the corresponding observational data when we take into account the joint efect of baroclinity and relief. It is also established that the consideration of the snow turbulent diffusion process leads to the higher quality of reproducing the wind velocity and friction stress in the atmospheric surface layer.

The sea ice belt in the South ocean near Antarctica is subject to considerable seasonal variations (from an abrupt extension in winter to the formation of open water in some places near the coast in summer). This substantially affects the albedo of the Earth surface and the processes of heat and mass exchange between the atmosphere and the ocean. In a period of the polar night the radiational cooling of the atmosphere over Antarctica results in the formation of a mainly high atmospheric pressure area here and a low pressure belt over the ocean. This pressure distribution is responsible for an advective heat and moisture transport in the upper and middle layers of the troposphere from the ocean to the continent, which is accompanied by stable catabatic winds (due to the dome-shaped relief of the Antarctic ice cover) in the atmospheric boundary layer. Every so often, a large amount of snow is transported from the continent to the ice-covered ocean, which also affects the processes of interaction between the atmosphere and the ocean [11] due to the increasing thickness of the snow cover. Moreover, snow particles suspended in the air flow change its characteristics, which results in an increase in the density of a (two-phase) medium, its temperature fall in the sublimation process, and an increase in the catabatic wind speed. The first two factors were studied, for example, in [20], the role of snow transport in turbulent momentum exchange with the underlying surface was considered in [22].

The parameterization problem of the processes in the boundary layer in high latitudes in models of atmospheric general circulation requires further experimental investigation and their modelling. For example, so far the parameters of sea ice,

---

complex relation between its extension and atmospheric circulation, the processes of interaction between radiation, cloudiness and turbulence in the stably stratified boundary layer have been poorly understood; moreover, blowing snow rather frequently complicates these processes. The works on modelling the boundary layer in the polar regions are still largely of a methodical character, which is mainly due to scanty experimental data.

However, it should be mentioned that by now several *in situ* experiments have been carried out with the aim to study the processes over and under the Antarctic ice shelf, including the winter period in the southern hemisphere. For example, we might mention the studies conducted under the Project 'Weddell Sea in winter' in 1986 [12], under the Soviet-German Project 'Investigation of the Weddell circulation' in 1989 [3], and under the analogous program in the Expedition ANTARCTICA X/4 in 1992 [8]. It turned out that because of a large difference in temperature between the atmosphere and the ocean the interaction between them in the above region is of an extremely dynamical character, which is reflected, in particular, in a sufficiently unusual structure of near-surface turbulence [10].

The present work is devoted to the study of processes over the surface of the Antarctic ice shelf by a one-dimensional baroclinic boundary layer model based on its earlier version [9]. The calculations of radiation and phase heat influxes are made using this model; besides, the model takes into account the processes of interaction between the atmosphere and the ice-covered ocean as well as the effects of near-surface snow transport [22]. In the present work particular emphasis has been placed on the so-called joint effect of baroclinicity and relief (JEBAR – the term which was first introduced by Sarkisyan [19]). The point is that the measurement data obtained in the Expedition ANTARCTICA X/4 was used in the numerical experiments with the model. Though these measurements were made over the horizontal surface of the ice-covered ocean, it is necessary to take into account that the motion in the observation region could have a catabatic component due to the Antarctic relief. Therefore the JEBAR could manifest itself in the atmospheric boundary layer over the ice shelf.

1. MODEL DESCRIPTION

All the calculations in this work are carried out by the 1.5th-order closure model. However, this model includes baroclinic and orographic effects by parameterically taking into account background (in the free atmosphere) processes.

1.1. Basic equations of the model

We take the Cartesian coordinates x, y, and z in which the x-axis is directed eastward, the y-axis is directed northward, and the z-axis is directed vertically upward. We write the equations for the atmospheric boundary layer as

$$\frac{\partial u}{\partial t} + \tilde{w}\frac{\partial u}{\partial z} = \frac{\partial}{\partial z}K\frac{\partial u}{\partial z} + fv - \tilde{p}_x/\tilde{\rho} \qquad (1.1)$$

$$\frac{\partial v}{\partial t} + \tilde{w}\frac{\partial v}{\partial z} = \frac{\partial}{\partial z}K\frac{\partial v}{\partial z} - fu - \tilde{p}_y/\tilde{\rho} \tag{1.2}$$

$$\frac{\partial \vartheta}{\partial t} + u\tilde{\vartheta}_x + v\tilde{\vartheta}_y + \tilde{w}\frac{\partial \vartheta}{\partial z} = \alpha_t\frac{\partial}{\partial z}K\frac{\partial \vartheta}{\partial z} + Q_r + Q_f \tag{1.3}$$

$$\frac{\partial q}{\partial t} + u\tilde{q}_x + v\tilde{q}_y + \tilde{w}\frac{\partial q}{\partial z} = \alpha_t\frac{\partial}{\partial z}K\frac{\partial q}{\partial z} + E - C \tag{1.4}$$

$$\frac{\partial q_w}{\partial t} + u\tilde{q}_{wx} + v\tilde{q}_{wy} + \tilde{w}\frac{\partial q_w}{\partial z} = \alpha_t\frac{\partial}{\partial z}K\frac{\partial q_w}{\partial z} - E + C - P \tag{1.5}$$

$$\frac{\partial p}{\partial z} = -g\rho \tag{1.6}$$

$$p = \rho RT, \quad \rho = \rho_a(1 + 0.61q - q_w) \tag{1.7}$$

$$\vartheta = T\left(\frac{p_0}{p}\right)^{R/c_p} \tag{1.8}$$

where u, v, and w are wind velocity components along the x-, y-, and z-axes, respectively; ϑ is the potential temperature related to the absolute temperature T by (1.8); q is specific humidity; q_w is the total specific water content that includes liquid and solid (ice) phases; p is pressure; ρ_a is the dry air density; ρ is the density of a air-water vapour-water-ice mixture; $(\tilde{p}_x, \tilde{p}_y)$, $(\tilde{\vartheta}_x, \tilde{\vartheta}_y)$, $(\tilde{q}_x, \tilde{q}_y)$, $(\tilde{q}_{wx}, \tilde{q}_{wy})$ are the components of the horizontal gradients of pressure, potential temperature, specific humidity, and water content in the free atmosphere; $\tilde{w}$ is a large-scale vertical velocity; Q_r and Q_f are radiation and phase heat influxes; C and E are the phase transition rate of water vapour→liquid drop fraction (condensation), water and ice→water vapour (evaporation/sublimation), respectively; P is the precipitation rate; K is the coefficient of the turbulent viscosity; α_t is the value characterizing the ratio of the turbulent diffusion coefficient to the coefficient of turbulent viscosity (which is calculated simultaneously with the calculation of near-surface turbulent flows by the Monin-Obukhov similarity theory [15]); R is the universal gas constant; c_p is the specific heat capacity of air at a constant pressure; $p_0 = 1000$ hPa is the standard value of pressure; $f = 2\Omega\sin\varphi$ is the Cariolis parameter (Ω is the angular velocity of the Earth rotation, φ is the latitude), g is the acceleration of gravity.

The turbulence coefficient K is related to the kinetic turbulent energy b and its dissipation rate ε by the Kolmogorov relation [7]

$$K = \frac{C_k b^2}{\varepsilon} \tag{1.9}$$

where C_k is a dimensionless constant. To calculate the values of b and ε, in the model we use the additional prognostic equations

$$\frac{\partial b}{\partial t} + \tilde{w}\frac{\partial b}{\partial z} = \alpha_b \frac{\partial}{\partial z} K \frac{\partial b}{\partial z} + K\left[\left(\frac{\partial u}{\partial z}\right)^2 + \left(\frac{\partial v}{\partial z}\right)^2 - \beta\frac{\partial \vartheta_v}{\partial z}\right] - \varepsilon \tag{1.10}$$

$$C_1 \frac{b}{\varepsilon}\left(\frac{\partial \varepsilon}{\partial t} + \tilde{w}\frac{\partial \varepsilon}{\partial z}\right) = C_1 \alpha_b \frac{b}{\varepsilon}\frac{\partial}{\partial z} K \frac{\partial \varepsilon}{\partial z} + K\left[\left(\frac{\partial u}{\partial z}\right)^2 + \left(\frac{\partial v}{\partial z}\right)^2 - \beta\frac{\partial \vartheta_v}{\partial z}\right] - \varepsilon. \tag{1.11}$$

Here $\vartheta_v = (1 + 0.61q - q_w)\vartheta$ is the virtual potential temperature; $\beta = g/\vartheta_{v0}$ is a buoyancy parameter (ϑ_{v0} is the reference value of ϑ_v); $\alpha_b = 0.73$. The dimensionless parameter C_1 is chosen as in [1]

$$C_1 = \left[1 + 0.69\frac{2-\mathcal{C}}{\sqrt{Re}}\right] \Big/ \mathcal{C}, \quad Re = \frac{(2b/3)^2}{\nu\varepsilon} \tag{1.12}$$

where ν is the molecular air viscosity and $\mathcal{C}$ is the universal constant (taken to be 1.9 in the model).

The following relation holds for the atmosphere to a sufficient accuracy:

$$Q_f = \frac{\mathcal{L}}{c_p}(C - E) \tag{1.13}$$

where $\mathcal{L}$ is the latent heat evaporation. This allows us [13] to rewrite equations (1.3)–(1.5) in terms of the 'conservative variables' $\vartheta_l = \vartheta - (\mathcal{L}/c_p)q_w$ (modification of the equivalent potential temperature) and $q_t = q + q_w$ (total moisture content)

$$\frac{\partial \vartheta_l}{\partial t} + u\tilde{\vartheta}_{lx} + v\tilde{\vartheta}_{ly} + \tilde{w}\frac{\partial \vartheta_l}{\partial z} = \alpha_t \frac{\partial}{\partial z} K \frac{\partial \vartheta_l}{\partial z} + Q_r \tag{1.14}$$

$$\frac{\partial q_t}{\partial t} + u\tilde{q}_{tx} + v\tilde{q}_{ty} + \tilde{w}\frac{\partial q_t}{\partial z} = \alpha_t \frac{\partial}{\partial z} K \frac{\partial q_t}{\partial z} - P \tag{1.15}$$

where the values $\tilde{\vartheta}_l$ and $\tilde{q}_t$ are related to $\tilde{\vartheta}$, $\tilde{q}$, and $\tilde{q}_w$ in an obvious way. The identity holds:

$$\vartheta + (\mathcal{L}/c_p)q \equiv \vartheta_l + (\mathcal{L}/c_p)q_t.$$

We emphasize that though we use a one-dimensional approximation, the model does take into account the processes of advective heat and moisture transport through the use of the parameters (the values tilded) which characterize the background (in the free atmosphere) motion.

1.2. Cloudiness and radiation

The regions, where specific humidity is larger than its saturation value, can form in the atmospheric boundary layer at certain values of temperature and pressure. Due to the condensation of water vapour there occurs cloudiness which substantially changes radiation properties. In this work we restrict our consideration to stratiformis clouds only, and for their calculation we use the algorithm proposed in [9].

In order to separate the value q_w into specific water content and ice content we use the empirical dependences [18] based on processing the flight measurements data in clouds [13]

$$q_w = q_l + q_i \tag{1.16}$$

$$q_l = f_l(T)q_w, \quad q_i = f_i(T)q_w, \quad f_l + f_i = 1 \tag{1.17}$$

$$f_l(T) = 0.0059 + 0.9941 e^{-a_0(T-273.2)^2} \tag{1.18}$$

where $a_0 = 0.003102 \ (^\circ C)^{-2}$.

The evolution of the atmospheric boundary layer over the ice-covered ocean is also appreciably specified by radiation processes represented in equation (1.3) by the term Q_r. Without going into details we point out that the model proposed in [6] was used to calculate long-wave and short-wave radiation fluxes. Along with the description of the effects of water vapour, ozone, and carbon dioxide (no other gases or aerosol were considered) we take into account the albedo of clouds and the underlying surface as well as the cloud amount when calculating radiation fluxes. The computational domain for radiation is extended to include the height corresponding to the p-surface with the value of the pressure $10\,\text{hPa}$. The profiles of temperature and specific humidity in the atmospheric boundary layer are taken from the solution of the problem and then extended to include the free atmosphere according to their climatic gradients. The vertical distributions of carbon dioxide and ozone concentrations are also given as climatic gradients over the whole computational domain.

1.3. Boundary conditions

The constant flux layer is isolated in the model, and its height h_1 is taken to be the lower boundary of the computational domain. Using the Monin-Obukhov similarity theory [15], we calculate the momentum flux τ_0, the heat flux H_0, and the moisture flux E_0 in this layer by the aerodynamical method

$$\boldsymbol{\tau}_0 \equiv -\left(\rho K \frac{\partial \mathbf{V}}{\partial z}\right)_{z=h_1} = -\rho_{h_1} C_D |\mathbf{V}_{h_1}| \mathbf{V}_{h_1} \tag{1.19}$$

$$H_0 \equiv -c_p \alpha_t \left(\rho K \frac{\partial \vartheta}{\partial z}\right)_{z=h_1} = -c_p \rho_{h_1} C_H |\mathbf{V}_{h_1}| (\vartheta_{h_1} - \vartheta_0) \tag{1.20}$$

$$E_0 \equiv -\alpha_t \left(\rho K \frac{\partial q}{\partial z} \right)_{z=h_1} = -\rho_{h_1} C_H |\mathbf{V}_{h_1}| (q_{h_1} - q_0) \tag{1.21}$$

where the subscript h_1 denotes the values of quantities at the upper boundary of the constant flux layer $z = h_1$, and the subscript 0 denotes those at a level of the underlying surface (to be exact for $z = z_0$, where z_0 is the surface roughness parameter). In formulae (1.19)–(1.21) we designate: $\mathbf{V} = (u, v)$. The drag coefficient C_D and the coefficient of heat and moisture exchange (the Stanton number C_H) are calculated by the relations

$$C_D = \varkappa^2 \left[\ln \left(\frac{z}{z_0} \right) - \psi_M(z/L) \right]^{-2} \tag{1.22}$$

$$C_H = \alpha_t \varkappa^2 \left[\ln \left(\frac{z}{z_0} \right) - \psi_M(z/L) \right]^{-1} \left[\ln \left(\frac{z}{z_{0t}} \right) - \psi_H(z/L) \right]^{-1} \tag{1.23}$$

where $\varkappa$ is the Karman constant, z_{0t} is a roughness parameter for heat (and moisture), and L is the Monin-Obukhov scale given by the relation

$$L = -\frac{u_*^3}{\varkappa B_0}. \tag{1.24}$$

Here $u_* = (|\tau_0|/\rho)^{1/2}$ is the friction velocity, $B_0 = \beta[H_0 + \vartheta_{v0}(0.61E_0 - W_0)]$ is a near-surface buoyancy flux (W_0 is the turbulent flux of the total specific water content). The universal functions ψ_M and ψ_H depend on stratification.

The exchange processes in the atmospheric near-surface layer and in the ice cover of the ocean result from the complex interaction between these media, and the integral expression for this interaction is a heat balance equation at their interface. The heat balance equation has the form

$$H_0 + \mathcal{L}E_0 - G_0 = R_0 \tag{1.25}$$

where R_0 is the radiation balance of the underlying surface and G_0 is a heat flux through ice from the ocean to the atmosphere. The air temperature at roughness level is assumed to coincide with the ice surface temperature $T_0 = T_{si}|_{z=0}$, the specific humidity has the saturation value $q_0 = q_{max}(T_0)$. To calculate a temperature profile in the ice cover $T_{si}(z)$ (the z-axis is directed upward) we use the heat equation

$$c_i \rho_i \frac{\partial T_i}{\partial z} = \frac{\partial}{\partial z} \lambda_i \frac{\partial T_i}{\partial z} \tag{1.26}$$

where ρ_i, c_i, and λ_i are the density, the specific heat, and the heat conductivity coefficient of sea ice, respectively. In this case $G_0 = -(\lambda_i \partial T_i/\partial)|_{z=0}$. Both the specific

heat and the heat conductivity coefficient depend on the temperature T_i and the local salinity of ice, S_i. To calculate them we use the empirical relations [14, 21]

$$\rho_i c_i = (\rho_i c_i)_0 \left[1 + \frac{a_1 S_i}{(T_i - 273.2)^2} \right] \tag{1.27}$$

$$\lambda_i = \lambda_{i0} \left[1 + \frac{a_2 S_i}{T_i - 273.2} \right] \tag{1.28}$$

where $(\rho_i c_i)_0 = 1.88 \times 10^5 \, \text{W s m}^{-3} \, \text{deg}^{-1}$, $\lambda_{i0} = 2.03 \, \text{W m}^{-1} \text{deg}^{-1}$, $a_1 = 9.1 (^\circ \text{C})^2$, $a_2 = 57.6^\circ$ C. The temperature at the lower boundary of ice is considered to coincide with the temperature of the ocean surface, which is obtained from the observations.

Let us now discuss the formulation of the lower boundary condition for the turbulent flux of the total specific water content W_0. We assume that a liquid water flux over ice is absent. However, in the case of drifting snow there occurs a specific ice content flux proportional to the turbulent flux of the concentration of airborne snow particles.

The equation for the mass concentration of snow particles, S, can be written [4] as

$$K \frac{\partial S}{\partial z} = -w_s \left(S - S_{h_1} \right) \tag{1.29}$$

where $S = \rho_s q_i / \rho_i$; ρ_s and ρ_i are snow and ice densities, respectively; w_s is the falling velocity of particles; S_{h_1} is the value of S determined by precipitations from the first model level.

With the unlimited supply of snow particles, the so-called limiting saturation regime on the underlying surface can be realized [4]. Under this regime the flow absorbs the maximum permissible (at its given parameters) amount of suspension so that it is not necessary to take the concentration of the particles on the surface as the boundary condition. The necessary condition for this regime to exist is

$$\omega = \frac{w_s}{\varkappa u_*} < 1. \tag{1.30}$$

When this condition is satisfied, the velocity distribution obeys the logarithmic law as is the case in a flow without suspension, but the value $\varkappa \omega$ instead of the constant $\varkappa$ appears in it.

In the more general case the boundary condition for the concentration of particles on the surface is assumed to be specified by the saltation process [2, 16] which occurs when the dynamic velocity u_* is larger than a threshold value u_{*t} below which the cohesion forces between particles prevent their escape from the surface.

By the hypothesis proposed in [16] a saltation layer forms so that shear friction stress on the surface is held close to the threshold value thus providing the possibility

for particles to escape and be in motion. In [16] the expression for the horizontal particle flux Q_s is derived using this hypothesis

$$Q_s = \int_{z_0}^{h_s} Su\,\mathrm{d}z = \mu u_*^3 (1 - u_{*t}^2/u_*^2)/g \tag{1.31}$$

$$\mu(\omega) = 0.25 \left(1 + \frac{4}{3} \varkappa\omega \right) \tag{1.32}$$

where h_s is the saltation layer thickness. Assuming that in this layer the profile $u(z)$ obeys the logarithmic law and the concentration is independent of the height $S(z) \equiv S_0$, we can obtain the expression for S_0 which can be used as the boundary condition for equation (1.29):

$$S_0 = \mu \frac{u_*^2}{\varkappa g z_0} \frac{1 - u_{*t}^2/u_*^2}{1 + \xi(\ln\xi - 1)} \tag{1.33}$$

where $\xi = h_s/z_0$. In [16] it was proposed that under the saltation conditions the roughness parameter must depend on the value of the friction velocity as is the case over the ocean in the case of developed undulation. Processing the experimental data [5] confirmed this hypothesis. It is also logical to assume that the analogous dependence holds for the saltation layer thickness. On this basis we take in the model:

$$z_0 = \gamma \frac{u_*^2}{g} \tag{1.34}$$

where γ (as well as the above parameter ξ) is a dimensionless constant. Following [5] we take the value of γ to be equal to 0.00132 and use the relation ξ for the value $\xi = 2\gamma^{-1}$.

We now formulate the lower boundary conditions for the kinetic turbulent energy b and its dissipation rate ε. By the Monin-Obukhov similarity theory [15], for $z = h_1$ we assume that

$$\varepsilon = \frac{u_*^3}{\varkappa h_1} \varphi_\varepsilon \left(\frac{h_1}{L} \right), \qquad b = u_*^2 \sqrt{\frac{\varphi_\varepsilon(h_1/L)}{C_k \varphi_M(h_1/L)}}. \tag{1.35}$$

For the normalized dissipation rate φ_ε we use the expression from [17]:

$$\varphi_\varepsilon(\zeta) = \varphi_M(\zeta) - \zeta.$$

To conclude this subsection we write the upper boundary conditions. It is assumed that the time variation of all the mean values for $z = h_2$ is known and the turbulent fluxes of kinetic turbulent energy and its dissipation rate are absent so that

$$u = u_{h_2}(t), \qquad v = v_{h_2}(t), \qquad \vartheta = \vartheta_{h_2}(t), \qquad q = q_{h_2}(t), \qquad q_w = q_{h_2}(t)$$

$$K\frac{\partial b}{\partial z} = 0, \quad K\frac{\partial \varepsilon}{\partial z} = 0 \tag{1.36}$$

where the values with subscript h_2 are obtained by the linear interpolation of the corresponding observational data.

2. RESULTS OF THE NUMERICAL EXPERIMENTS

The observed data used in this work embraces an 18-hour period from 4 a.m. to 10 p.m. (Greenwich Mean Time) on June 21, 1992 when the German research ice-breaker 'Polarstern' was almost in the stationary position (8.04° W.L., 70.54° S.L.) in the ices of the Weddell Sea near the Antarctic coast. In the whole analysed period a wind was blowing from the northeast sector. After 9 a.m. the meteorological conditions near the underlying surface were characterized by an abrupt deterioration of visibility caused by drifting snow. The ice cover thickness was 0.8 m in the period studied.

As the initial conditions for the experiments discussed in this section, we use the vertical distributions of the variables, which result from the profile interpolation on the model grid. The profiles were observed at 4 a.m. GMT on June 21, 1992:

$$u(z,0) = u_{\text{obs}}(z,0), \quad v(z,0) = v_{\text{obs}}(z,0)$$

$$\vartheta(z,0) = \vartheta_{\text{obs}}(z,0), \quad q(z,0) = q_{\text{obs}}(z,0). \tag{2.1}$$

The observations of the specific water content and the turbulence measurements above the constant flow layer were not made. Therefore it was taken that at the initial instant $q_w(z,0) \equiv 0$. To calculate the profiles of turbulent kinetic energy and the dissipation rate we used equations (1.10) and (1.11) in the stationary approximation. In the intervals between the measurements the values with subscript 'obs' were obtained by the linear interpolation between two adjacent observation intervals. To calculate the pressure gradient components in equations (1.1) and (1.2) we used the geostrophic relations

$$\tilde{p}_x/\tilde{\rho} = fv_g, \quad \tilde{p}_y/\tilde{\rho} = -fu_g \tag{2.2}$$

where the observed profiles of the wind velocity components in the free atmosphere (above 2 km) are used as u_g and v_g.

Recall that though the observations of the parameters of the atmospheric boundary layer were made over the horizontal surface of the ice-covered ocean, the Antarctic relief could affect the current in the studied region through its catabatic component. In the first rather rough approximation this effect can be taken into account by the expression for a 'large-scale' vertical velocity:

$$\tilde{w} = z_{sx}u_g + z_{sy}v_g$$

where $z_s(x,y)$ is a function describing the relief.

We carried out the numerical experiments of two types. The experiments of the first type were to demonstrate the effect of baroclinicity and relief in interaction between the atmosphere and the Antarctic ice shelf. In experiment 1 (the barotropic case) we assumed that

$$u_g(t) = u_{obs}(h_2, t), \qquad v_g(t) = v_{obs}(h_2, t)$$

$$z_{sx} = z_{sy} = \tilde{\vartheta}_{lx} = \tilde{\vartheta}_{ly} = \tilde{q}_{tx} = \tilde{q}_{ty} = 0. \tag{2.3}$$

In experiment 2 (the baroclinic case) we used linear extrapolations for the geostrophic wind components

$$u_g = u_{obs}(h_2, t) + \left.\frac{\partial u_{obs}}{\partial z}\right|_{z=h_2}(z - h_2)$$

$$v_g = v_{obs}(h_2, t) + \left.\frac{\partial v_{obs}}{\partial z}\right|_{z=h_2}(z - h_2). \tag{2.4}$$

To calculate the background temperature gradients we used the thermal wind relations

$$\tilde{\vartheta}_x = \frac{f\vartheta_{obs}}{g}\left[\frac{\partial v_g}{\partial z} + \frac{g(1 + R/c_p)}{RT_{obs}}v_g\right]$$

$$\tilde{\vartheta}_y = -\frac{f\vartheta_{obs}}{g}\left[\frac{\partial u_g}{\partial z} + \frac{g(1 + R/c_p)}{RT_{obs}}ug\right]. \tag{2.5}$$

Besides, the effect of the relief was not taken into account in experiment 2 either and it was assumed that $q_{wx} = q_{wy} = 0$ and

$$\tilde{q}_x = \frac{\partial}{\partial x}\left[rq_{max}(\tilde{T}, \tilde{p})\right] \approx r\frac{\partial q_{max}(\tilde{T}, \tilde{p})}{\partial x} \approx r\frac{\partial q_{max}}{\partial \tilde{T}}\frac{\partial \tilde{T}}{\partial x}$$

$$\approx r\frac{\partial q_{max}}{\partial \tilde{T}}\left(\tilde{\vartheta}_x + \frac{f}{c_p}v_g\right) \tag{2.6}$$

where $r = q/q_{max}$ is relative humidity. Similarly,

$$\tilde{q}_y \approx r\frac{\partial q_{max}}{\partial \tilde{T}}\left(\tilde{\vartheta}_y - \frac{f}{c_p}u_g\right). \tag{2.7}$$

Experiment 3 was analogous to experiment 2, but the joint effect of baroclinicity and relief was taken into account. In this case we put $z_{sx} = 0.001$, $z_{sy} = 0$.
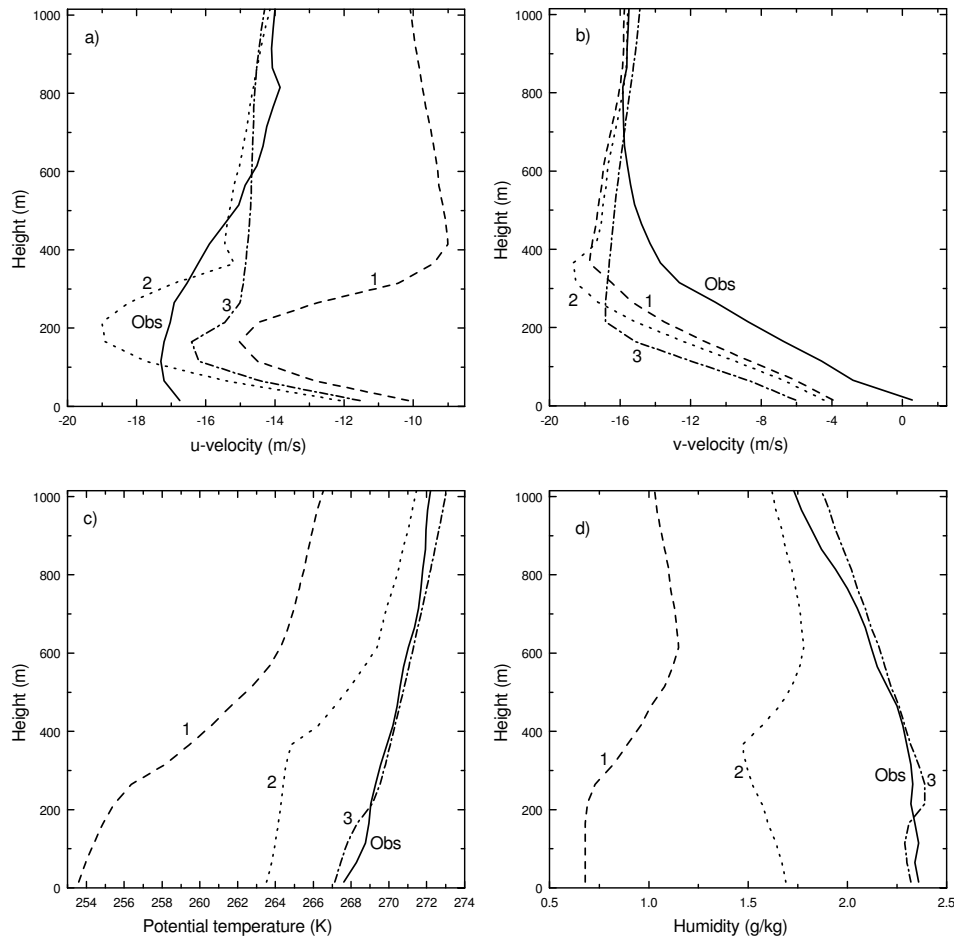
Figure 1. Comparison between the calculated (dotted curves with numbers corresponding to the experiment number) at the final instant of integration and observed (solid line marked 'Obs') vertical profiles of the atmospheric boundary layer characteristics: (a) zonal velocity component, (b) meridional velocity component, (c) potential temperature, (d) specific humidity.

In the experiments of the second type we studied the effect of the near-surface snow transport. All the calculations in these experiments were carried out in a baroclinic approximation (experiment 3 was regarded as a reference one). To calculate the snow concentration in the saltation layer in experiment 4 we used relation (1.33). In experiment 5 the underlying surface was regarded as an infinite particle source. In both experiments the particle size was taken to be 0.06 mm, the falling velocity was $w_s = 0.15$ m/s.

Figure 1 shows the results of a comparison between the observed (solid line marked 'Obs') and calculated (dotted lines with numbers corresponding to the experiment number) profiles of the zonal velocity component (Fig. 1a), the meridional velocity component (Fig. 1b), potential temperature (Fig. 1c), and specific humidity
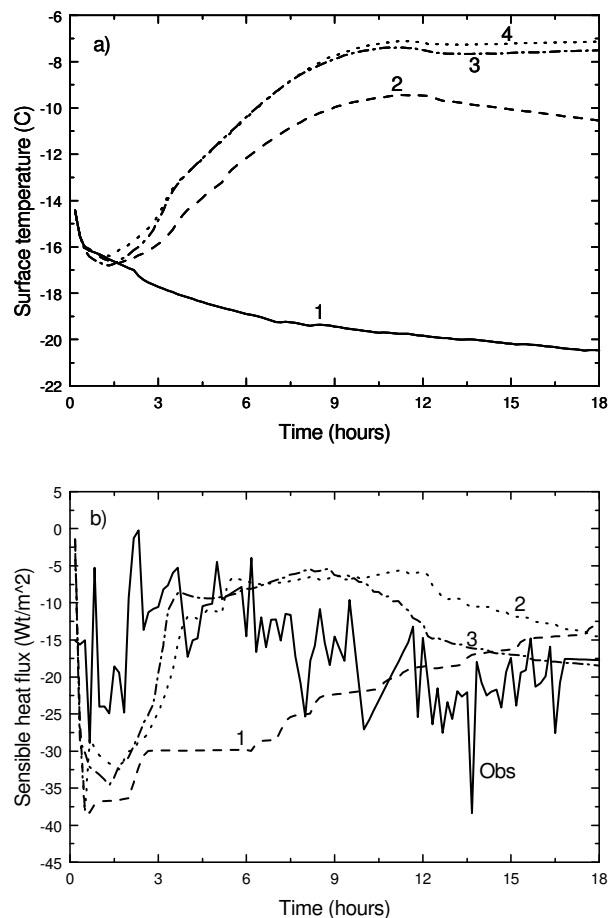
Figure 2. Time variation of: (a) calculated temperature of the underlying surface, (b) sensible heat flux observed at a height of 15 m (solid line), and the flux calculated by the experimental data. Numbers on the curves correspond to the experiment number.

(Fig. 1d) at the final instant of model integration (18 hours). As seen from Figs. 1c and 1d, there occurs a consistent improvement of the temperature and the specific humidity reproduction quality as compared to that in the barotropic case (curves 1). The best agreement is obtained in the experiment which takes into account the JEBAR (curves 3): the differences are not larger than $0.8°$ C in absolute value for temperature and 0.2 g kg^{-1} for specific humidity. Ignoring the orographic contribution (curves 2) has most dramatic effects on the lower 600 m thick layer.

Figure 2a shows the time variations of temperature of the underlying surface, which were calculated in various experiments. In the barotropic case (curve 1) in the whole period studied the (radiation) cooling of the ice surface from $-14°$ C to $-20°$ C occurs, while the atmospheric lower layer becomes increasingly stable and the near-surface sensible heat flux (Fig. 2b, curve 1) systematically decreases (in ab-

solute value) not compensating for the radiation cooling. The direct measurements by an acoustic thermometer-anemometer (Fig. 2b, solid curve), in general, demonstrate the opposite pattern. Taking account of the background flow baroclinicity and the associated horizontal heat and moisture advection reverses the time variation of temperature on the ice surface (Fig. 2a, curve 2): on the whole it increases and reaches $-10.5°$ C by the end of integration. The inclusion of the orographic effect results in a further increase in temperature on the underlying surface by $3°$ C (Fig. 2a, curve 3). The time variation of the sensible heat flux in both 'baroclinic' experiments (Fig. 2b, curves 2 and 3) is in good agreement with its observed behaviour. We also note that in the 18-hour period studied one temperature measurement at the 'atmosphere-snow/ice' interface (at the instant corresponding to 5 hours of the model time) was made: it turned out to be close to $-12°$ C and essentially coincided with the value obtained in experiment 3.

We now consider the vertical profiles of the horizontal velocity components. As seen from Fig. 1b, the model distribution of the meridional velocity component does not depend strongly on the experimental conditions: its maximum values (in absolute value) are obtained in the layer from 200 m to 400 m. The difference between them is not larger than 2 m/s but on the average they are more than the observed values by a factor of 1.5. Figure 1a shows that the observed profile of the zonal velocity in the lower 400 m layer has the configuration of the form of a jet flow, which is characteristic of catabatic wind. In the numerical experiments this configuration is most pronounced, the difference in the extrema between the results of experiments 1 and 2 being 4 m/s. The best agreement with *in situ* data is obtained in the experiment with allowance for the JEBAR (curve 3). Near the underlying surface the numerical results in experiment 3 and the aerological measurement data differ dramatically (the differences reach 5 m/s and are comparable with those obtained for the meridional velocity).

Figure 3a presents the time variation of the modulus of the wind velocity at a height of 15 m, which is measured by an acoustic thermometer-anemometer (solid curve), as compared to that calculated in experiments 3, 4, and 5 (dotted curves with the corresponding numbers). In the variability of the observed wind speed we can distinguish two regimes: wind intensification from 8 m/s to 16 m/s during the first 7 hours and then its slight decreasing to 12 m/s, its subsequent value being 14 m/s. Experiment 3, in general, reproduces this pattern. However, the maximum value of the speed is about 5 m/s less than the observed one. By the end of the model integration time the difference decreases to 1–2 m/s, which is substantially less than the differences with the aerological data whose quality is known to be the lowest near the Earth surface.

In addition, Fig. 3 shows the numerical results in experiments 4 and 5 which take into account the effects of snow transport caused by blowing snow. This factor manifests itself in the atmospheric surface layer only. As seen from Fig. 3a, the best agreement with the observed data is obtained in experiment 5 in which the snow surface is regarded as an infinite particle source [4]. The calculated maximum value of the velocity modulus at the stage of wind intensification differs from the observed data only by 2 m/s. At the final stage of the model integration (last 6 hours) the
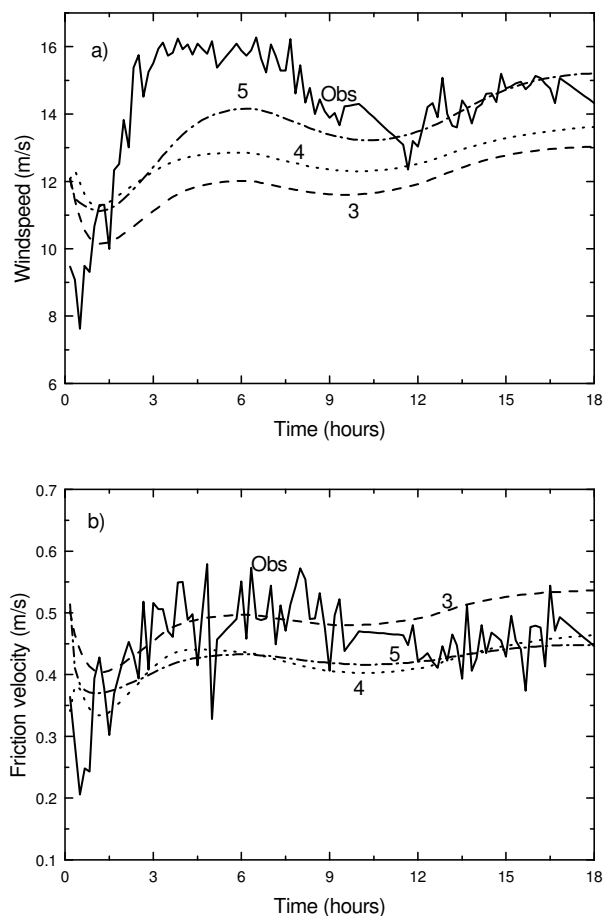
Figure 3. Comparison between the calculated (dotted lines with numbers corresponding to the experiment number) and observed (solid line marked 'Obs') time variations at a height of 15 m: (a) wind speed, (b) friction velocity.

model calculations and (smoothed) measurement results essentially coincide with one another. The results for the case in which the particle source on the surface 'turned on' only if the friction velocity was higher than a threshold value are located (curve 4) between the results of experiments 3 and 5. Figure 3b shows the time variation of the friction velocity u_* calculated by the direct measurement data at a height of 15 m (solid line) as compared to that calculated in experiments 3, 4, and 5 (dotted lines with the corresponding numbers). Curves 4 and 5 in this figure little differ from each other but differ essentially from those obtained in experiment 3, thus demonstrating the known effect of decreasing friction in suspension fluxes (see, e.g. [4, 22]), which is accompanied by the surface wind intensification (Fig. 3a). Unlike the wind speed, the underlying surface temperature is not affected by the presence of air-suspended snow particles (Fig. 2a, curves 3 and 4).

3. CONCLUSION

As an example we took the situation, which existed on June 21, 1992 (in a period of the polar night) near the coast of Antarctica and was characterized by a strong advective heat and moisture transport from the ocean to the continent, and studied the part played by the joint effect of baroclinicity and relief (JEBAR) and the processes of snow transport in interaction between the atmospheric boundary layer and the ice shelf. The problem of this kind is of great interest for the purpose of parameterization of the atmospheric boundary layer in the polar regions in global climate models. This is because under the conditions of frequently observed highly stable density stratification the turbulent transport processes become substantially weaker. The numerical experiments performed showed that under certain conditions the horizontal large-scale temperature and specific humidity gradients and the associated baroclinic flow in the free atmosphere (forcing for the boundary layer) are responsible for this advective heat and moisture transport which can compensate for the radiation cooling processes and maintain the effective turbulent exchange between the atmosphere and the ice-covered ocean. It is also established that the inclusion of the catabatic component of the vertical velocity, which is due to the relief of Antarctica, substantially improves the reproduction of the characteristics of the atmospheric boundary layer by the one-dimensional model even if the underlying surface is horizontal. This is a peculiar manifestation of the JEBAR first described by Sarkisyan (see, e.g. [19]) for the ocean dynamics problems. The experiments, which take into account blowing snow when suspended snow particles are present in the atmosphere, showed that under conditions studied the above factor affects only the atmospheric surface layer and substantially improves the reproduction of the wind speed and the friction stress. At the same time the underlying surface temperature and the sensible heat flux turn out to be not very sensitive to these changes.

Acknowledgements

I am indebted to Academician A. S. Sarkisyan for his willingess to impart his scientific knowledge and knowledge of the world to his colleagues. The data used in this work was obtained in collaboration with Dr. C. Wamser at the Institute of Polar and Marine Research (Bremerhaven, Germany). I am grateful to him for fruitful discussions of the issues concerning the atmospheric boundary layer in the polar regions.

REFERENCES

1. B. Aupoix, J. Cousteau, and J. Liandart, MIS: a way to derive the dissipation equation. *Turbulent Shear Flows* (1989) **6**, 6–17.

2. R. A. Bagnold, *The Physics of Blown Sand and Desert Dunes*. W. Morrow, New York, 1941.

3. N. V. Bagryantsev and A. V. Klepikov, International winter expedition in the region of the Weddel Sea circulation (1989). *Information bulletin of the Russian Antarctic Expedition*, 1994, No. 118, pp. 13–23 (in Russian).

4. G. I. Barenblatt and G. S. Golitsyn, Local structure of mature dust storms. *J. Atmos. Sci.* (1975) **31**, 1917–1933.

5. A. C. Chamberlain, Roughness length of sea, sand, and snow. *Boundary-Layer Meteorol.* (1983) **25**, 405–409.

6. D. Harshvardhan, D. Roger, D. A. Randall, and T. G. Corsetti, A fast radiation parameterization for atmospheric circulation models. *J. Geophys. Res.* (1987) **92**, 1009–1016.

7. A. N. Kolmogorov, Equations of turbulent motion of an incompressible fluid. *Izv. Akad. Nauk SSSR Ser. Phizicheskaya* (1942) **6**, 56–58 (in Russian).

8. P. Lemke, The expedition ANTARCTICA X/4 of R/V 'Polarstern' in 1992, with contributions of the participants. *Berichte zur Polarforschung* (1994), No. 140.

9. V. N. Lykossov and G. A. Platov, A numerical model of interaction between atmospheric and oceanic boundary layers. *Russ. J. Numer. Anal. Math. Modelling* (1992) **7**, No. 5, 419–440.

10. V. N. Lykossov and C. Wamser, Turbulence intermittency in the atmospheric surface layer over snow-covered sites. *Boundary-Layer Meteorol.* (1995) **72**, 393–409.

11. D. H. Male, The seasonal snowcover. In: *S. Colbeck, Dynamics of Snow and Ice Masses.* Academic, New York, 1980, pp. 305–395.

12. D. Martison and C. Wamser, Ice drift and momentum exchange in winter antarctic pack ice. *Geophys. Res.* (1990) **95**, 1741–1755.

13. L. T. Matveev, *Cloud Dynamics.* Gidrometeoizdat, Leningrad, 1981 (in Russian).

14. G. A. Maykut and N. Untersteiner, Some results from a time dependent, thermodynamic model of sea ice. *J. Geophys. Res.* (1971) **76**, 1550–1575.

15. A. S. Monin and A. M. Obukhov, Main regularities of turbulent mixing in the atmospheric surface layer. *Trudy Geofiz. Inst. Akad. Nauk SSSR* (1954) **151**, No. 24, 163–187 (in Russian).

16. P. Owen, Saltation of uniform grains in air. *J. Fluid Mech.* (1964) **20**, 225–242.

17. H. A. Panofsky and J. A. Dutton, *Atmospheric Turbulence. Models and Methods for Engeneering Applications.* Wiley-Interscience Publ., New York, 1984.

18. B. Rockel, E. Raschke, and B. Weyres, A parameterization of broad band radiatve transfer properties of water, ice and mixed clouds. *Contr. Phys. Atmos.* (1991) **64**, 1–12.

19. A. S. Sarkisyan, *Numerical Analysis and the Prediction of Sea Currents.* Gidrometeoizdat, Leningrad, 1977 (in Russian).

20. R. A. Schmidt, Transport rate of drifting snow and the mean wind speed profile. *Boundary-Layer Meteorol.* (1986) **34**, 213–241.

21. N. Untersteiner, Natural desalination and equilibrium salinity profile of perennial sea ice. *J. Geophys. Res.* (1968) **73**, 1251–1257.

22. C. Wamser and V. N. Lykossov, On the friction velocity during blowing snow. *Contr. Phys. Atmos.* (1995) **68**, 85–94.